ChemComm

COMMUNICATION

View Article Online
View Journal | View Issue

Membrane analysis with amphiphilic carbon dots†

Sukhendu Nandi,[a] Ravit Malishev,[a] Kaviya Parambath Kootery,[a] Yelena Mirsky,[b] Sofiya Kolusheva[b] and Raz Jelinek*[ab]

Cite this: *Chem. Commun.*, 2014, **50**, 10299

Received 9th May 2014,
Accepted 18th July 2014

DOI: 10.1039/c4cc03504f

www.rsc.org/chemcomm

Newly-synthesized amphiphilic carbon dots were used for spectroscopic analysis and multicolour microscopic imaging of membranes and live cells. We show that Förster resonance energy transfer (FRET) occurred from the amphiphilic carbon dots to different membrane-associated fluorescence acceptors. The amphiphilic carbon dots enabled imaging of membrane disruption by the beta-amyloid peptide.

Carbon dots are small (<10 nm), quasi-spherical nanoparticles,[1–3] and have attracted significant interest due to their unique structural and photophysical properties and applications in nanobiotechnology.[3–15] Carbon dots could be particularly advantageous for biological studies since they are biocompatible and potentially less cytotoxic than semiconductor dots, chemically stable, and their broad excitation/emission spectral range and low photobleaching are beneficial for imaging applications. We report a readily-applicable synthetic procedure for large-scale preparation of carbon dots in which the graphitic core is coated with hydrocarbon layers. We show for the first time that the amphiphilic carbon dots incorporate into *membrane bilayers*. Notably, the membrane-associated carbon dots can function as energy donors in Förster resonance energy transfer (FRET) processes having significantly different excitation wavelengths. The amphiphilic carbon dots were further employed as vehicles for analysis and visualization of membrane interactions and bilayer reorganization by known membrane-active species and could be inserted into cells for multicolour imaging applications.

Fig. 1 depicts the synthesis scheme and morphological features of the amphiphilic carbon dots. Preparation of the carbon dots was carried out in an aqueous solution, starting with *O*,*O*′-di-lauroyl tartaric acid anhydride (**1**) produced through reacting L-tartaric acid with lauryl chloride (Fig. 1).[16]

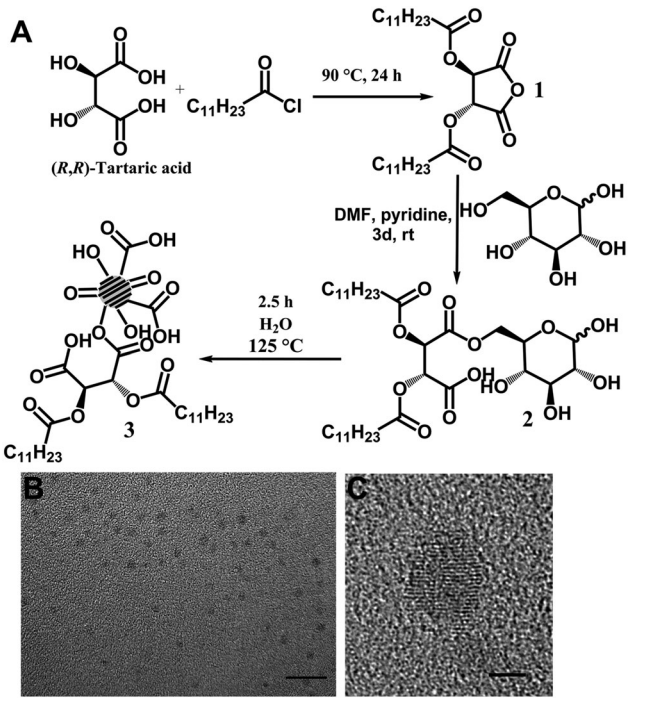

Fig. 1 Synthesis and structures of the amphiphilic carbon dots. (A) Synthesis scheme; (B) high-resolution transmission electron microscopy (HRTEM) image of a carbon dot sample. Scale bar is 10 nm; (C) HRTEM image of a single amphiphilic carbon dot, showing the crystal planes. Scale bar is 2 nm.

The anhydride **1** was then subsequently reacted with D-glucose, yielding 6-*O*-acylated fatty acid ester of D-glucose (**2**).[16] The final step consists of carbonization of glucose and simultaneous *in situ* self-passivation yielding carbon dots (**3**) exhibiting inner graphitic cores[17] coated with an amphiphilic layer comprising alkyl chains and carboxylic acid moieties (full experimental details are provided in the ESI† file, Fig. S1–S4). Significantly, the new synthetic procedure does not require additional surface passivation, common in most published schemes as a necessary step to prevent aggregation. Overall, the synthesis procedure is

[a] *Department of Chemistry, Ben Gurion University of the Negev, Beer Sheva 84105, Israel. E-mail: razj@bgu.ac.il; Fax: +972-8-6472943*
[b] *Ilse Katz Institute for Nanotechnology, Ben Gurion University of the Negev, Beer Sheva 84105, Israel*

† Electronic supplementary information (ESI) available: ^{1}H NMR, FT-IR, XRD, statistical analysis of particle sizes, and cell viability. See DOI: 10.1039/c4cc03504f

simple, utilizes inexpensive, widely-available carbon precursors, and yields large quantities of carbon dots (up to several grams per batch of starting materials). Using quinine sulfate as a reference, the quantum yield of carbon dots was found to be 16.5%, 9.4%, and 4.7% in chloroform, hexane, and NaH_2PO_4 buffer, respectively, which is higher (in chloroform) than many previous reports.[18]

^{1}H NMR (Fig. S5 and S6, ESI†) confirms the transformation of the glucose residues into elemental carbon and the presence of coating alkyl chains, while Fourier-transform infrared spectroscopy (FT-IR, Fig. S7, ESI†) provides evidence for the formation of graphitic carbon coated with hydrocarbon chains. Notably, as outlined in Fig. 1A, the synthetic procedure utilizes readily available and inexpensive reagents. Statistical analysis based upon the high-resolution transmission electron microscopy (HRTEM) results in Fig. 1B indicates that the particles have a relatively narrow size distribution between 1.5 and 3.0 nm exhibiting a mean diameter of 2.3 ± 0.3 nm (Fig. S8, ESI†). The HRTEM image of a representative amphiphilic carbon dot in Fig. 1C underscores the crystallinity of the graphite core of the nanoparticles.[19,20] X-ray diffraction analysis (Fig. S9, ESI†) yields an interlayer spacing of 0.46 nm, consistent with previous reports.[21]

To investigate membrane association of the amphiphilic carbon dots we compared the photoluminescence (PL) properties of the amphiphilic carbon dots in *phosphate buffer vs. incubation with giant vesicles* (GVs) comprising egg phosphatidylcholine (egg PC), designed to mimic membrane environments (Fig. 2A and B).[22] Specifically, Fig. 2A depicts the excitation-dependent PL spectra of the amphiphilic carbon dots in phosphate buffer, while the comparable PL spectra of the dots incubated with GVs are shown in Fig. 2B. The wide PL range (*i.e.* multicolour emission) apparent in both graphs is one of the signature properties of carbon dots, and has been ascribed to size variations of the nanoparticles,[4,21] distinct emissive traps at the carbon dot surface[4,21] or related mechanisms.[4]

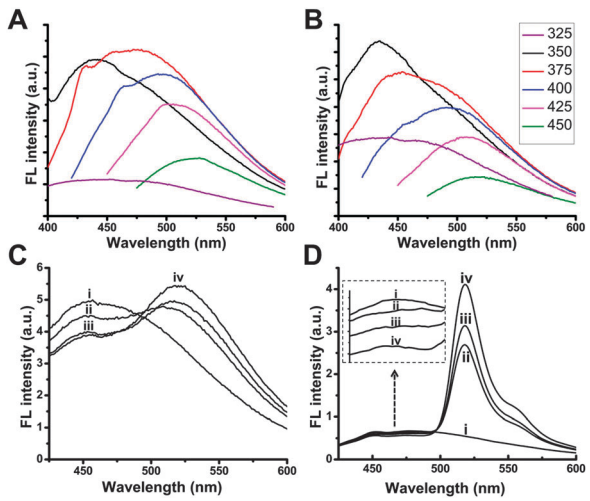

Fig. 2 Photophysical properties of amphiphilic carbon dots in membrane vesicles. (A) and (B) Photoluminescence spectra of carbon dots excited at different wavelengths, recorded in phosphate buffer (A), and in solutions of giant lipid vesicles (B). (C) and (D) FRET occurring upon mixing amphiphilic carbon dots (energy donors) with GVs containing fluorescent acceptors: (C) PC : NBD-PE (100 : 1 mole ratio). The numerals (i)–(iv) correspond to different concentrations of the fluorescent acceptor dye: (i) 3.3 mg mL^{-1} carbon dots (no GVs present); (ii) 3.3 μM NBD-PE; (iii) 5 μM NBD-PE; (iv) 6.6 μM NBD-PE. (D) PC:BODIPY-PH (1000 : 1 mole ratio). The numerals (i)–(iv) correspond to different concentrations of the fluorescent acceptor dye: (i) 0.1 mg mL^{-1} carbon dots (no GVs present); (ii) 0.05 μM BODIPY-PH; (iii) 0.1 μM BODIPY-PH; (iv) 0.2 μM BODIPY-PH. The inset depicts a magnification of the fluorescent spectra indicated by the arrow (between 420 nm and 490 nm).

Importantly, Fig. 2B shows that the GVs modulate the PL spectra, giving rise to changes in the *relative intensities* of excitation/emission curves. Specifically – in *buffer* the maximum emission intensity was induced upon excitation at 375 nm, while in the *membrane environment* the maximum emission occurred upon excitation at a *different* wavelength (350 nm). Furthermore, an experimentally-significant blue shift of around 30 nm was apparent between the emission spectrum recorded upon excitation at 375 nm in buffer and upon incubation of the amphiphilic carbon dots with GVs. The difference in photoluminescence profiles in Fig. 2A and B reflects the influence of the vesicle environment on the carbon dots' optical properties, and is indicative of carbon dot insertion into the lipid bilayer.

Förster resonance energy transfer (FRET) experiments depicted in Fig. 2C and D provide further insight into bilayer insertion of the amphiphilic carbon dots, and also point to utilization of the carbon dots as energy donors in a broad spectral range. In the experiments summarized in Fig. 2C and D we recorded FRET from the carbon dots to two membrane-associated dyes exhibiting significantly different excitation/emission wavelengths: *N*-(7-nitrobenz-2-oxa-1,3-diazol-4-yl)1,2-dihexadecanoyl-*sn-glycero*-3-phosphoethanolamine (NBD-PE; excitation maximum 469 nm, emission maximum 540 nm) and 4,4-difluoro-8-(2-(2-((1,3-dioxoisoindolin-2-yl)oxy)acetamido)phenyl)-1,3,5,7-tetramethyl-4-bora-3*a*,4*a*-diaza-*s*-indacene-phthalamide (BODIPY-PH; excitation maximum 500 nm, emission maximum 510 nm).[23] In the FRET analyses, we prepared giant vesicles comprising egg PC, and NBD-PE or BODIPY-PH. We then titrated the dye-containing GVs into solutions having a constant (final) concentration of the amphiphilic carbon dots. Following brief incubation, the GV–carbon dot solutions were excited at wavelengths in which the emission of the amphiphilic carbon dots coincides with the excitation of the specific acceptor dye embedded within the GVs (thus achieving optimal FRET). Specifically, in the case of NBD-PE, the carbon dot–GV solution was excited at 370 nm (in which the carbon dot emission peak was at around 450 nm, Fig. 2B), while the solution containing GVs incorporated into BODIPY-PH was excited at 390 nm, in which the carbon dots emit at around 485 nm (Fig. 2B).

The fluorescence results in Fig. 2C and D confirm the occurrence of energy transfer from the amphiphilic carbon dots to the membrane-embedded dyes. In the case of NBD-PE (Fig. 2C), increasing the concentration of NBD-PE/PC GVs resulted in an increase of the NBD fluorescence emission at around 540 nm, while in parallel a decrease of the carbon dot fluorescence emission at around 450 nm was apparent. These peak intensity modulations are ascribed to the occurrence of FRET between the amphiphilic carbon dots and the bilayer-embedded dye. The FRET data recorded after addition of BODIPY-PH/egg PC GVs to the amphiphilic carbon dots (Fig. 2D) yielded a comparable

outcome as the NBD-PE/PC vesicles. Specifically, an experimentally-significant increase in the BODIPY-PH emission peak (515 nm) was recorded upon excitation at 390 nm – the excitation of the carbon dots (acting as fluorescence donors) – and elevating the concentration of the BODIPY-PH/PC GVs. The enhanced emission of BODIPY-PH was accompanied by a decrease in the carbon dot emission at around 485 nm, due to the FRET. Quantification of the FRET efficiencies further demonstrates that the extent of energy transfer depends upon the carbon dot: acceptor ratios (Fig. S10 and S11, ESI†). It should be noted that similar FRET processes involving semiconductor dots were reported.[24,25] The observation of FRET from the amphiphilic carbon dots to two distinct dyes is significant, as it demonstrates that the broad PL range of the carbon dots (*i.e.* Fig. 2B) enables energy transfer to varied fluorescent acceptors exhibiting different excitation/emission profiles.

The photoluminescence properties of the amphiphilic carbon dots make possible microscopic imaging applications. Fig. 3 presents confocal microscopy images of GVs after incubation with amphiphilic carbon dots. Multicolour imaging of the GVs is demonstrated in Fig. 3A using four distinct excitation/emission wavelengths. The fluorescence microscopy images in Fig. 3A indicate that the amphiphilic carbon dots were uniformly distributed within the vesicle bilayer. Fig. 3B vividly demonstrates the use of the amphiphilic carbon dots for real-time visualization of membrane processes. Fig. 3B presents microscopy images recorded at different times after addition of amyloid β (1–40) (Aβ40) to GVs labeled with the amphiphilic carbon dots (images obtained with additional excitation/emission wavelengths are shown in Fig. S12, ESI†). Aβ40 has been extensively studied as a prominent toxic factor in Alzheimer's disease and is believed to interact with membrane bilayers.[26–28] Indeed, the fluorescence microscopy images in Fig. 3B provide a dramatic visual demonstration of a gradual Aβ40-induced distortion of the spherical membrane surface, resulting in significantly deformed vesicle morphology. Imaging of membrane deformation following interactions with other membrane-active species was also recorded (Fig. S13, ESI†).

The spectroscopic and microscopic data in Fig. 2 and 3 underscore the significance of the broad excitation/emission range for membrane analysis. Indeed, while other fluorescent dyes or inorganic nanoparticles (*i.e.* semiconductor dots) exhibit specific excitation/emission wavelengths which generally depend upon the molecular properties (in case of fluorescent dyes) or the dot diameter and composition,[29,30] a single amphiphilic carbon dot sample displays multiple colours – of which one could select the desired wavelength for imaging and/or membrane analysis (using FRET to specific acceptor dyes, for example).

The amphiphilic carbon dots can also be employed as vehicles for live cell imaging (Fig. 4). In these experiments we prepared mixed small unilamellar vesicles comprising egg-PC and the amphiphilic carbon dots, and exploited endocytic vesicle-uptake by cells[31,32] as the mechanism for cell internalization of the carbon dots. The confocal microscopy images in Fig. 4 depict epithelial Chinese hamster ovary (CHO) cells following incubation with the egg-PC/carbon dot vesicles. The fluorescence images, recorded upon excitation at three different wavelengths, demonstrate that the carbon dots were inserted into the cells, exhibiting a relatively uniform distribution within the cytosol and nucleoli. Notably, carbon dot uptake by the cells did not seem to adversely

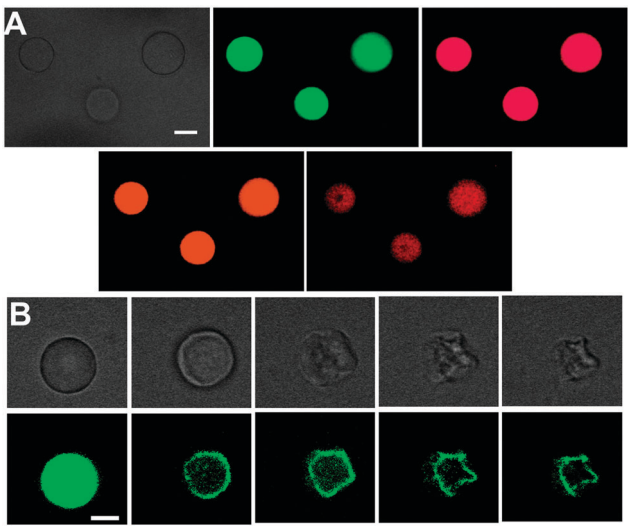

Fig. 3 Fluorescence imaging of giant vesicles labeled with the amphiphilic carbon dots. (A) Bright field microscopy (top left), and confocal fluorescence microscopy images recorded upon excitation using a 440 nm emission filter EM 477/45 (green); excitation using a 488 nm emission filter EM 525/50 (magenta); excitation using a 514 nm emission filter EM 525/50 (orange); excitation using a 568 nm emission filter EM 640/120H (red). Scale bar corresponds to 10 μm. B. Bright field (top) and fluorescent images (excitation at 440 nm) of giant vesicles labeled with the carbon dots following addition of Aβ40. From left: before addition (control); 1 min after addition; 10 min after addition; 20 min after addition and 1 h after addition. Scale bar corresponds to 5 μm.

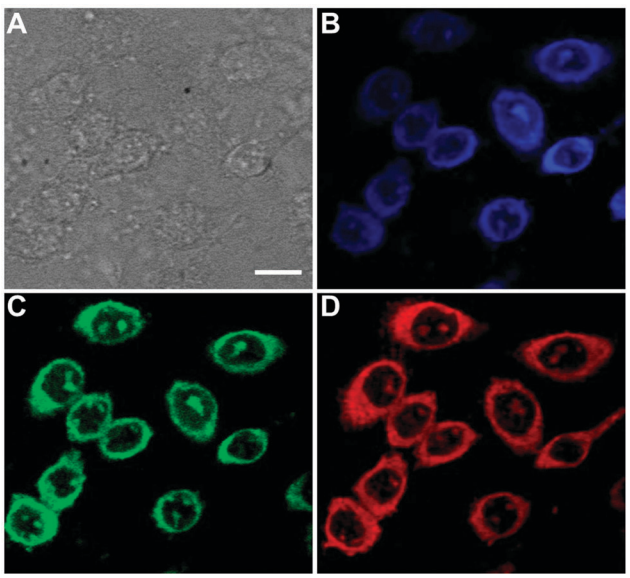

Fig. 4 Cell imaging with amphiphilic carbon dots. Bright-field image (A) and confocal fluorescence microscopy images of CHO cells incubated with egg-PC/carbon dot vesicles. The images were recorded upon excitation using a 405 nm emission filter 525/30 nm (B); excitation using a 488 nm emission filter 525/30 nm (C); excitation at 561 nm emission 641/40 nm (D). The fluorescence images confirm insertion of the carbon dots into the cells. Scale bar is 10 μm.

affect their viability as judged by cell shapes and application of cell viability assays (Fig. S14, ESI†). Similar to the giant vesicle imaging experiments (Fig. 3), the intrinsic multicolour properties of the carbon dots constitute a significant advantage for cell imaging applications.

In summary, we present a new synthetic route for production of carbon dots coated with an amphiphilic hydrocarbon layer, and demonstrate, for the first time, application of these amphiphilic carbon dots for analysis and imaging of biological membranes and membrane events. The newly-synthesized amphiphilic carbon dots exhibit notable advantages as membrane probes in comparison with other currently-used fluorescent markers and inorganic dots, since the intrinsically broad photoluminescence range of a single carbon dot sample makes possible multicolour imaging, and FRET to varied membrane-associated fluorophores. The bright multicolour luminescence of the carbon dots enables visualization of membrane interactions in model vesicle systems and microscopic imaging of live cells. Overall, this study indicates that amphiphilic carbon dots constitute a potentially powerful vehicle for investigating and visualizing membranes and membrane processes.

We are grateful to Dr David Sprinzak, Tel Aviv University, for help with the cell imaging experiments, and Vladimir Ezersky, Ilse Katz Institute for Nanotechnology, Ben Gurion University for help with the HR-TEM experiments. The Kreitman School of Advanced Graduate Studies at Ben Gurion University is acknowledged for financial support (SN).

Notes and references

1 Y. Xu, M. Wu, Y. Liu, X.-Z. Feng, X.-B. Yin, X.-W. He and Y.-K. Zhang, *Chem. – Eur. J.*, 2013, **19**, 2276–2283.
2 W. Kwon, S. Do and S.-W. Rhee, *RSC Adv.*, 2012, **2**, 11223.
3 S. N. Baker and G. A. Baker, *Angew. Chem., Int. Ed.*, 2010, **49**, 6726–6744.
4 J. Shen, Y. Zhu, X. Yang and C. Li, *Chem. Commun.*, 2012, **48**, 3686–3699.
5 L. Cao, X. Wang, M. J. Meziani, F. Lu, H. Wang, P. G. Luo, Y. Lin, B. A. Harruff, L. M. Veca, D. Murray, S.-Y. Xie and Y.-P. Sun, *J. Am. Chem. Soc.*, 2007, **129**, 11318–11319.
6 H. Li, Z. Kang, Y. Liu and S.-T. Lee, *J. Mater. Chem.*, 2012, **22**, 24230–24253.
7 X. Michalet, F. F. Pinaud, L. A. Bentolila, J. M. Tsay, S. Doose, J. J. Li, G. Sundaresan, A. M. Wu, S. S. Gambhir and S. Weiss, *Science*, 2005, **307**, 538–544.
8 S. Choi, R. M. Dickson and J. Yu, *Chem. Soc. Rev.*, 2012, **41**, 1867–1891.
9 S.-T. Yang, L. Cao, P. G. Luo, F. Lu, X. Wang, H. Wang, M. J. Meziani, Y. Liu, G. Qi and Y.-P. Sun, *J. Am. Chem. Soc.*, 2009, **131**, 11308–11309.
10 R. Liu, D. Wu, S. Liu, K. Koynov, W. Knoll and Q. Li, *Angew. Chem., Int. Ed.*, 2009, **48**, 4598–4601.
11 L. Cao, M. J. Meziani, S. Sahu and Y.-P. Sun, *Acc. Chem. Res.*, 2012, **46**, 171–180.
12 A. Salinas-Castillo, M. Ariza-Avidad, C. Pritz, M. Camprubí-Robles, B. Fernández, M. J. Ruedas-Rama, A. Megia-Fernández, A. Lapresta-Fernández, F. Santoyo-Gonzalez, A. Schrott-Fischer and L. F. Capitan-Vallvey, *Chem. Commun.*, 2013, **49**, 1103–1105.
13 W. Kwon and S.-W. Rhee, *Chem. Commun.*, 2012, **48**, 5256.
14 Z.-C. Yang, M. Wang, A. M. Yong, S. Y. Wong, X.-H. Zhang, H. Tan, A. Y. Chang, X. Li and J. Wang, *Chem. Commun.*, 2011, **47**, 11615.
15 C. Fowley, B. McCaughan, A. Devlin, I. Yildiz, F. M. Raymo and J. F. Callan, *Chem. Commun.*, 2012, **48**, 9361–9363.
16 S. Nandi, H.-J. Altenbach, B. Jakob, K. Lange, R. Ihizane, M. P. Schneider, Ü. Gün and A. Mayer, *Org. Lett.*, 2012, **14**, 3826–3829.
17 X.-H. Li, S. Kurasch, U. Kaiser and M. Antonietti, *Angew. Chem., Int. Ed.*, 2012, **51**, 9689–9692.
18 L. Tang, R. Ji, X. Cao, J. Lin, H. Jiang, X. Li, K. S. Teng, C. M. Luk, S. Zeng, J. Hao and S. P. Lau, *ACS Nano*, 2012, **6**, 5102–5110.
19 L. Tang, R. Ji, X. Li, K. S. Teng and S. P. Lau, *J. Mater. Chem. C*, 2013, **1**, 4908–4915.
20 W. Kwon, J. Lim, J. Lee, T. Park and S.-W. Rhee, *J. Mater. Chem. C*, 2013, **1**, 2002–2008.
21 S. Sahu, B. Behera, T. K. Maiti and S. Mohapatra, *Chem. Commun.*, 2012, **48**, 8835.
22 A. Moscho, O. Orwar, D. T. Chiu, B. P. Modi and R. N. Zare, *Proc. Natl. Acad. Sci. U. S. A.*, 1996, **93**, 11443–11447.
23 J. Rayo, N. Amara, P. Krief and M. M. Meijler, *J. Am. Chem. Soc.*, 2011, **133**, 7469–7475.
24 A. R. Clapp, I. L. Medintz, J. M. Mauro, B. R. Fisher, M. G. Bawendi and H. Mattoussi, *J. Am. Chem. Soc.*, 2003, **126**, 301–310.
25 G. Jiang, A. S. Susha, A. A. Lutich, F. D. Stefani, J. Feldmann and A. L. Rogach, *ACS Nano*, 2009, **3**, 4127–4131.
26 W. Gibson Wood, G. P. Eckert, U. Igbavboa and W. E. Muller, *Biochim. Biophys. Acta*, 2003, **10**, 281–290.
27 E. Sparr, M. F. Engel, D. V. Sakharov, M. Sprong, J. Jacobs, B. de Kruijff, J. W. Hoppener and J. A. Killian, *FEBS Lett.*, 2004, **577**, 117–120.
28 S. A. Kotler, P. Walsh, J. R. Brender and A. Ramamoorthy, *Chem. Soc. Rev.*, 2014, DOI: 10.1039/C3CS60431D.
29 W. Zheng, Y. Liu, A. West, E. E. Schuler, K. Yehl, R. B. Dyer, J. T. Kindt and K. Salaita, *J. Am. Chem. Soc.*, 2014, **136**, 1992–1999.
30 H. S. Wi, S. J. Kim, K. Lee, S. M. Kim, H. S. Yang and H. K. Pak, *Colloids Surf., B*, 2012, **97**, 37–42.
31 N. S. Parkar, B. S. Akpa, L. C. Nitsche, L. E. Wedgewood, A. T. Place, M. S. Sverdlov, O. Chaga and R. D. Minshall, *Antioxid. Redox Signaling*, 2009, **11**, 1301–1312.
32 D. Perrais and C. J. Merrifield, *Dev. Cell*, 2005, **9**, 581–592.

